

## CHAPTER 3

### RESULTS AND DISCUSSIONS

The results of gravity measurements, electrical resistivity sounding measurement and density measurement on rock samples obtained from the present study are presented in this chapter. The aim of this research is to determine regional subsurface geological of Vientiane basin.

#### 3.1. Density of rock samples

In the present study density measurement was conducted on 28 rock samples collected from 7 sites within the study area and 10 rock samples collected from 4 sites in Northeastern part of study area. All samples are Cretaceous sandstone and their locations are shown in Figure 3.1.

The results showed that density of Cretaceous sandstone within the study area ranges from 2.28 to 2.61 g/cm<sup>3</sup> with an average density of  $2.43 \pm 0.08$  g/cm<sup>3</sup> (Figure 3.2 (a)) and density of Cretaceous sandstone in Northeastern part of study area ranges from 2.39 to 2.50 g/cm<sup>3</sup> with an average density of  $2.45 \pm 0.04$  g/cm<sup>3</sup> (Figure 2.3 (b)). There is no difference in density of both two groups of sandstone. The density of two groups ranges from 2.28 to 2.61 g/cm<sup>3</sup> with an average density of  $2.43 \pm 0.07$  (Figure 3.2 (c))

Table 3.1: Average density of rock samples

Rock types	Average density (g/cm <sup>3</sup> )	Site number	Sample number	Location
Cretaceous Sandstone	$2.43 \pm 0.08$	7	28	Naxaythong and Xaithani districts
Cretaceous Sandstone	$2.45 \pm 0.04$	4	10	Northeastern part of study area

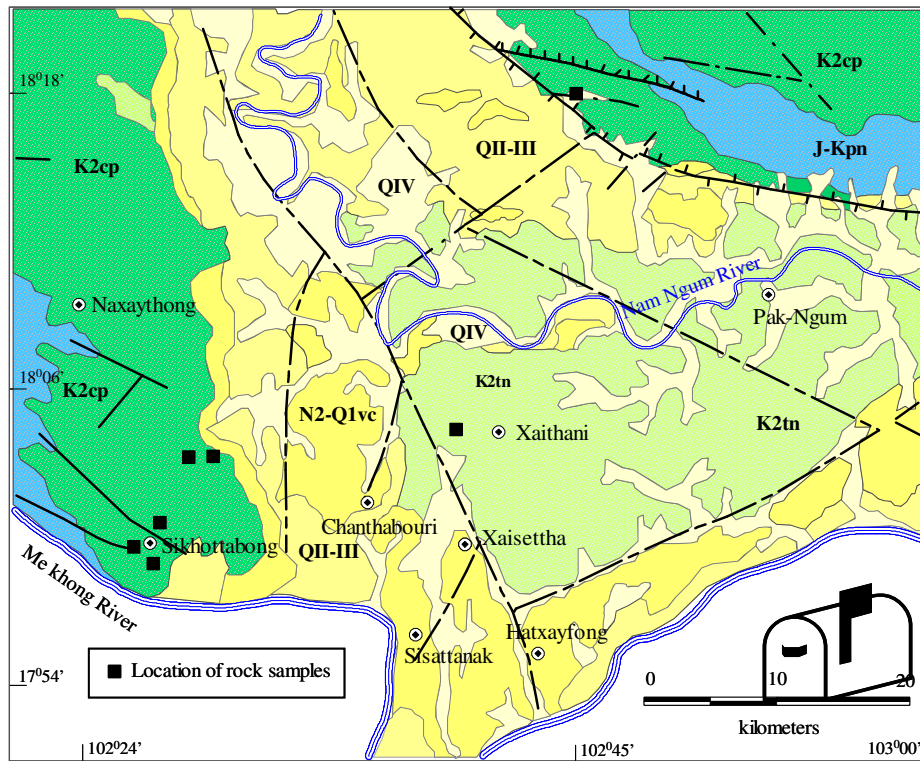


Figure 3.1 Locations of rock samples on geological map of Vientiane basin

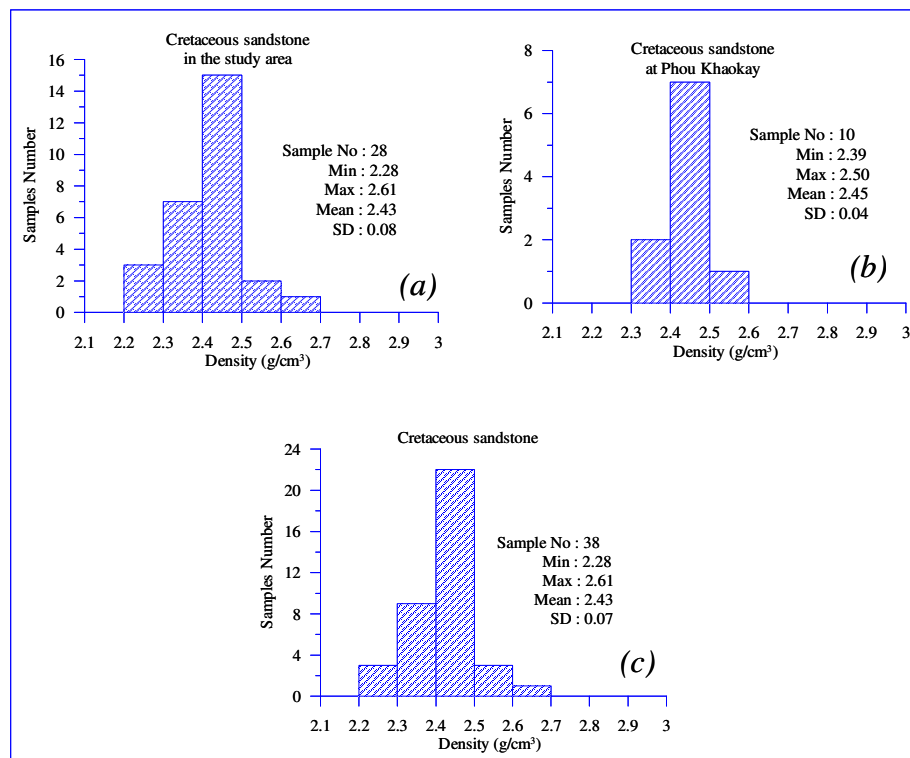
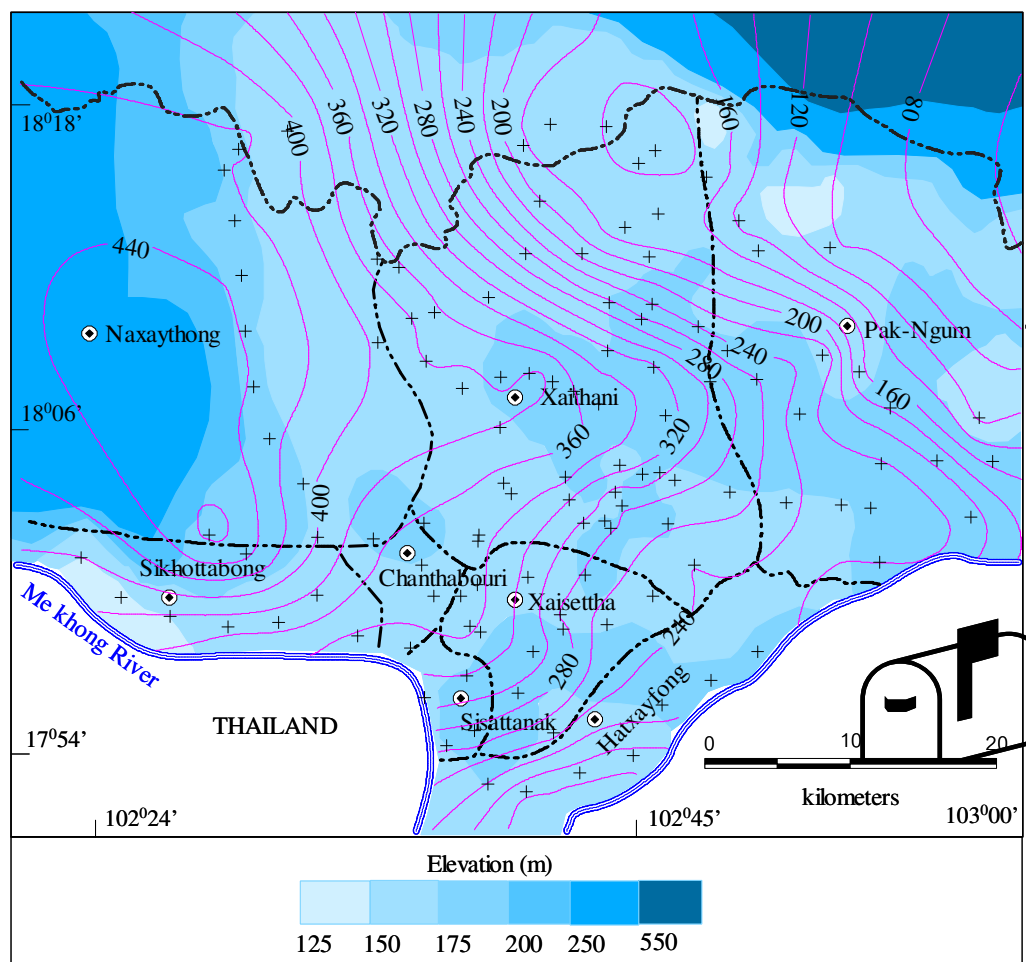


Figure 3.2 Density distribution of Cretaceous sandstone

### 3.2. Bouguer map of the study area

The main objective of gravity measurement is to determine regional subsurface geological structures of Vientiane basin. In the present work, geological structures such as faults and depth to basement rock will be determined by making use of available borehole data, VES-results and available geological map of the study area as constraints.



*Figure 3.3* Contour map of Bouguer anomalies overlies on topographic map of Vientiane basin (Contour interval of 20 g.u)

Generally, Bouguer anomaly of the study area ranges from 45 to 472 g.u. as shown in Figures 3.3 and 3.4. This Bouguer anomaly is independent from topography of the study area as shown in Figure 3.3. According to Bouguer anomaly map three distinct areas of different anomaly are identified as follows:

1. Area of high Bouguer anomaly. This area is in western part of the study area covering Chanthabouri, Sikhottabong and Naxaythong districts. Bouguer anomaly in this area ranges from 340 to 440 g.u. According to geological map, the surface rock in this area is Jurassic-Cretaceous rocks which comprise mainly sandstone and siltstone.
2. Area of moderate Bouguer anomaly. This is the area in the middle part of the study area covering areas of Xaithani, Xaisettha, Sisattanak and Hatxayfong districts. Its Bouguer anomaly ranges from 200 to 320 g.u. According to geological map, the surface rock in this area is Cretaceous rocks which comprise mainly claystone, siltstone, potash salt and rock salt.
3. Area of Low Bouguer anomaly. This area is in northeastern part of the study area, covering area of Pak-Ngum district and likely to extend eastward into Vientiane basin. Its Bouguer anomaly ranges from 60 to 180 g.u. According to geological map, the surface rock in this area is Jurassic-Cretaceous rocks which comprise mainly sandstone and siltstone. A very low gravity anomaly in this area indicated that density of subsurface rock is lower than other zones in the study area. Low gravity anomaly may be caused by increasing thickness of sediment in Vientiane basin on the east. Vientiane basin is the northwest extension of Sakon Nakhon basin in Thailand (Gardner *et al.*, 1967).

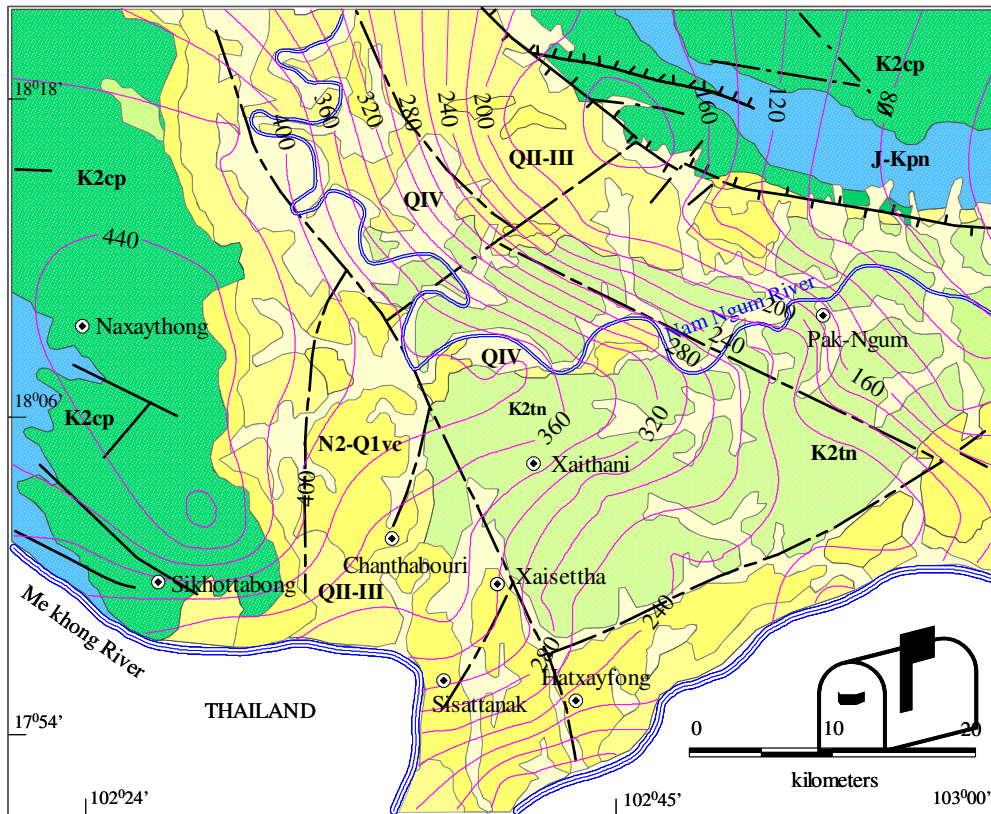


*Figure 3.4* Contour of Bouguer anomalies overlies on geological map of Vientiane basin (Contour interval of 20 g.u.)

Bouguer anomaly map superimposed on the geological map of the study area is shown in Figure 3.4. It can be observed that parallel contour lines of Bouguer anomaly in the northern part of the study area, northwest and northeast of Xaithani, follow very well with NW-SE faults proposed on the geological map. Similar agreement is observed in the middle part of the study area between Xaithani and Pak-Ngum districts, in the southern part of the study area, northwest to north of Hatxayfong. In addition, NE-SW fault in the southern part of the study area, northeast of Hatxaifong, also follows Bouguer anomaly contour lines. This indicates that Bouguer anomaly map obtained from the present study very well reflects subsurface geological structures of the study area.

### 3.3. Gravity modeling of Vientiane basin

In order to delineate subsurface geological structures in Vientiane basin, geophysical modeling was carried out on five west-east gravity profiles, as shown in Figure 3.5. Information on the geological map of the study area, such as surface rocks, locations of faults and the geological section on line CC' (Figure 3.6), is used as constraints for this modeling.

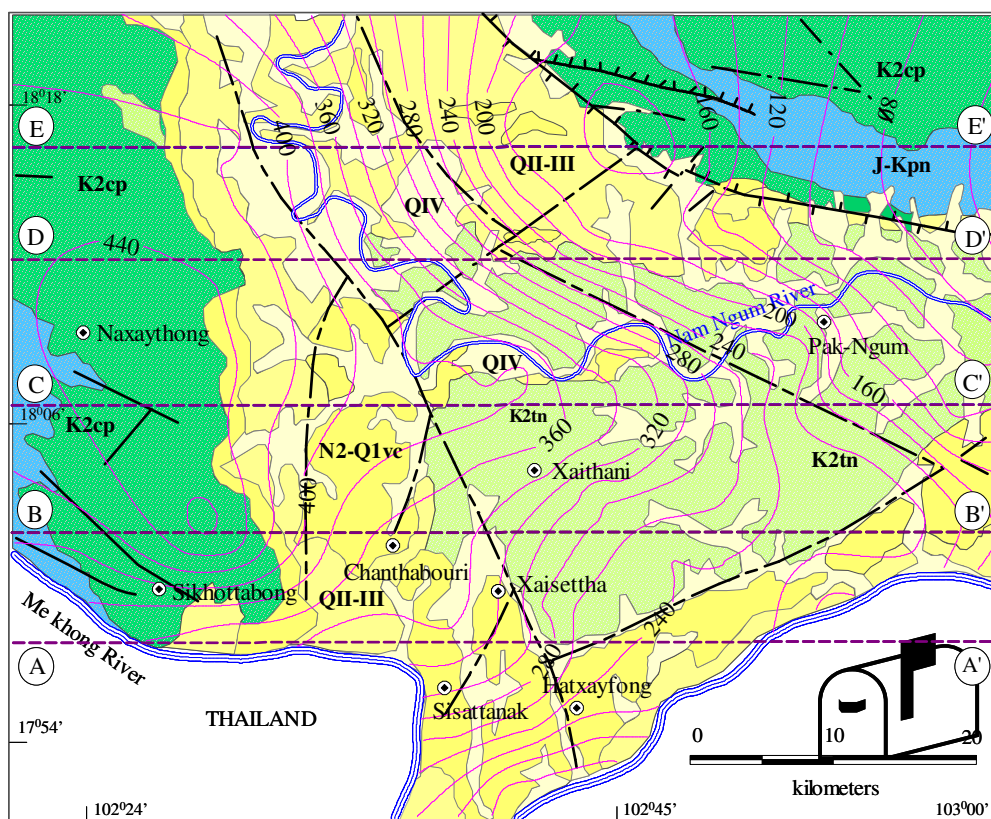


*Figure 3.5* Bouguer anomaly contours and locations of profiles AA', BB', CC', DD' and EE' on geological map of Vientiane basin

According to geological cross-section on line CC' (Figure 3.6), Cretaceous rocks which underlie Quaternary sediments is considered as basin sediments. The basin sediments of Cretaceous age comprise two formations, namely; Tha Ngon formation (K2tn) and Champa formation (K2cp). Tha Ngon formation comprises Na-salt, claystone, siltstone, sandstone, calcareous claystone bearing

siltstone, potash salt, gypsum and anhydrite, rhyolite and tuff, whereas Champa formation which underlies Tha Ngon formation consists of sandstone, siltstone, brownish sandstone, white arkose, quartz-feldspar sandstone.

The basins sediment of Cretaceous age overly Phu Pha Nang formation (J-Kpn) of Jurassic-Cretaceous age which crops out at the western end of line CC'. Phu Pha Nang formation comprises sandstone bearing mica, white siltstone and brown sandstone, quartzite sandstone. The Phu Pha Nang formation is thought to be underlain by Nam Sait formation (T3ns) of Triassic age which does not crop out in the western end of line CC'. The Nam Sait formation consists of black sandstone, siltstone and claystone bearing white mica, angular purplish clay, limestone and conglomerate.

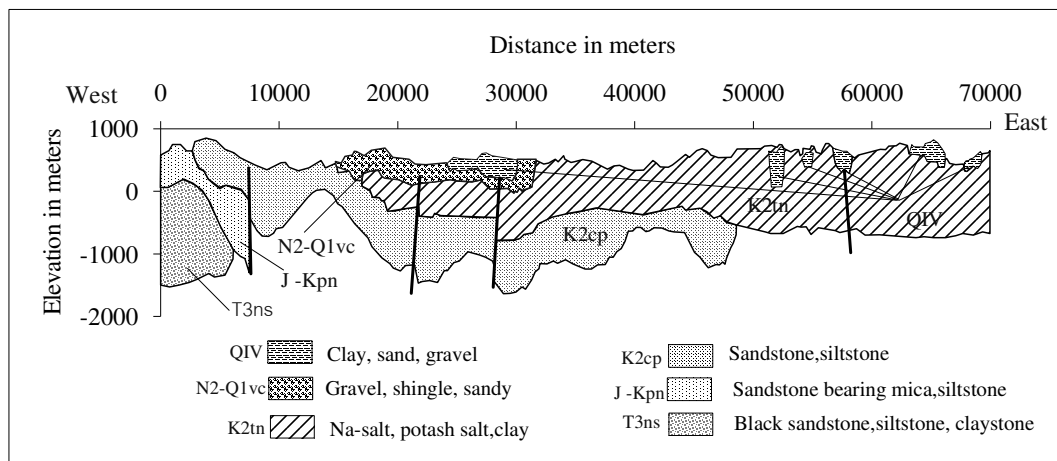


*Figure 3.6* Geological cross section of Vientiane basin on line CC' (modified from the geological map of Vientiane capital)

In geophysical modeling, the measured density of  $2.45\text{g/cm}^3$  was assigned for Cretaceous sandstone (K2cp) whereas assumed densities of 2.30 and  $2.70\text{g/cm}^3$  were assigned for Tha Ngon formation (K2tn) and Phu Pha Nang formation (J-Kpn) respectively. Phu Pha Nang formation together with underlying rocks are considered to be surrounding rock in this gravity modeling. In addition, a constant regional anomaly of 450 g.u in the study area was assumed and removed from observed Bouguer anomaly in all modeling profiles.

### 3.3.1 Line AA' (17°58'N)

Gravity anomaly and subsurface geological model of line AA' are shown in Figure 3.7 (b) and (c). Line AA' is at latitude 17°58'N and longitudes 102°21'E to 103°00'E and its length is about 70 kilometers. A decrease of Bouguer anomaly from about -98 g.u. on the western end of the profile to -248 g.u. on the eastern end of the profile with two sharp steps of decrease around distances 30,000 and 50,000 meters were clearly observed, as shown in Figure 3.7 (b). The surface geology in vicinity of line AA' is shown in Figure 3.7 (a). It can be observed that geological faults were also reported between distances 40,000 and 55,000 meters.

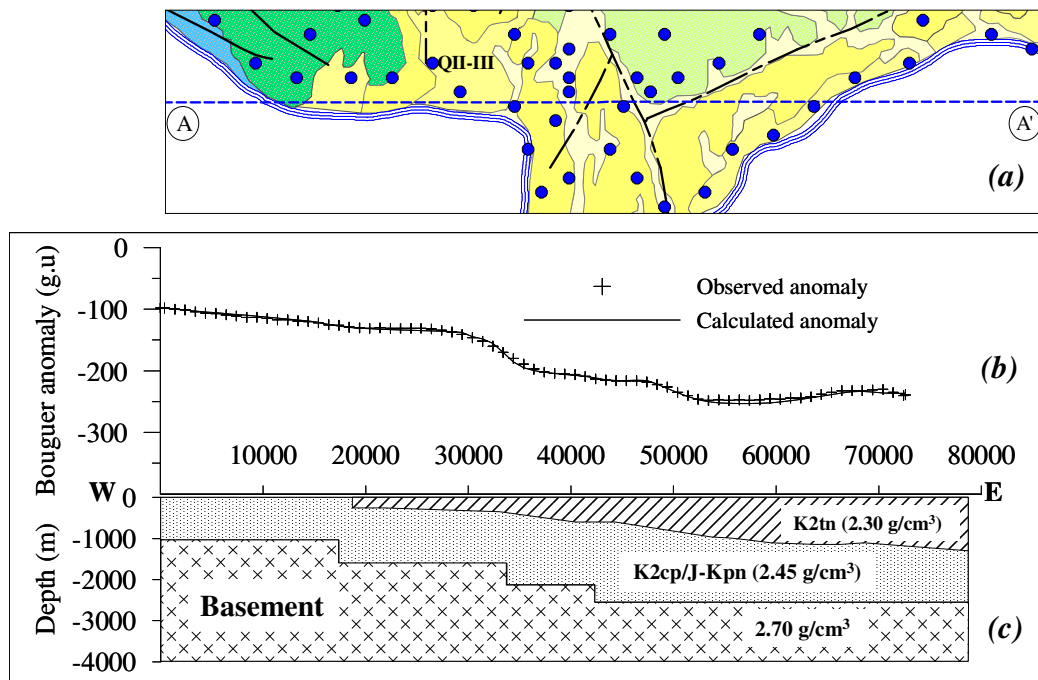


Figure 3.7 (a) Surface geological map in vicinity of line AA'  
 (b) Gravity anomaly on line AA'  
 (c) Geophysical model on line AA'

An increase in thickness of basin sediments of Cretaceous age from 1,000 meters on the western end to 2,800 meters on the eastern end with steps of change in thickness of basin sediments between distances 18,000 and 41,000 meters was modeled to explain the decrease of Bouguer anomaly on line AA' (Figure 3.7

(c)). In addition, a salt layer of 100 to 1,000 meters thick was modeled in the upper part of basin sediments to conform to subsurface geology of the study area.

### 3.3.2 Line BB' (18°02' N)

Gravity anomaly and subsurface geological model of line BB' are shown in Figure 3.8 (b) and (c). Line BB' is at latitude 18°02' N and longitudes 102°21' E to 103°00' E and its length is about 70 kilometers. An increase of Bouguer anomaly from about -40 g.u. on the western end of the profile to +20 g.u. at distance 10,000 meters, and follows by a decrease to -297 g.u. on the eastern end of the profile with steps of decrease around distances 17,000, 28,000 and 64,000 meters were clearly observed, as shown in Figure 3.8 (b). The surface geology in vicinity of line BB' is shown in Figure 3.8 (a). Geological faults of northwest-southeast and northeast-southwest trending were also reported between distances 20, 000 and 70,000 meters.

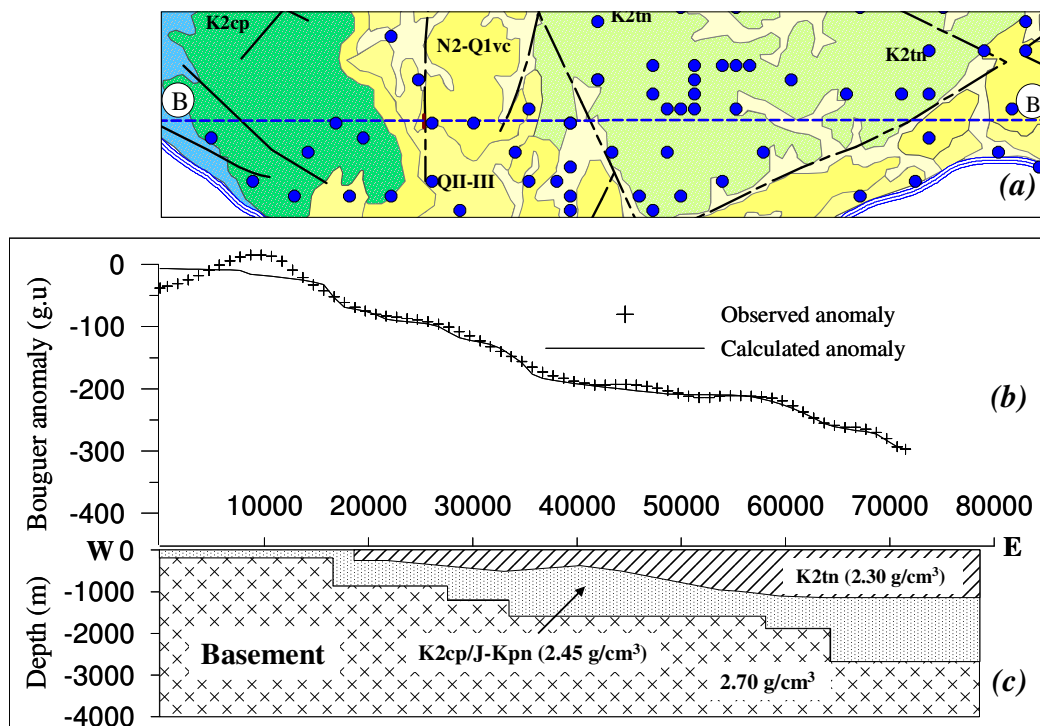


Figure 3.8 (a) Surface geological map in vicinity of line BB'  
 (b) Gravity anomaly on line BB'  
 (c) Geophysical model on line BB'

An increase in thickness of basin sediments of Cretaceous age from 200 meter at distance 0 meters on the western end to 3,000 meters on the eastern end with steps of change in thickness of basin sediments between distances 17,000 and 64,000 meters was modeled to explain the Bouguer anomaly on line BB' (Figure 3.8 (b)). Similarly, a salt layer of less than 1,000 meters thick was modeled in the upper part of basin sediments to conform to subsurface geology of the study area.

### 3.3.3 Line CC' (18°07'N)

Gravity anomaly and subsurface geological model of line CC' are shown in Figure 3.9 (b) and (c). Line CC' is at latitude 18°07'N and longitudes 102°21' E to 103°00' E and its length is about 70 kilometers.

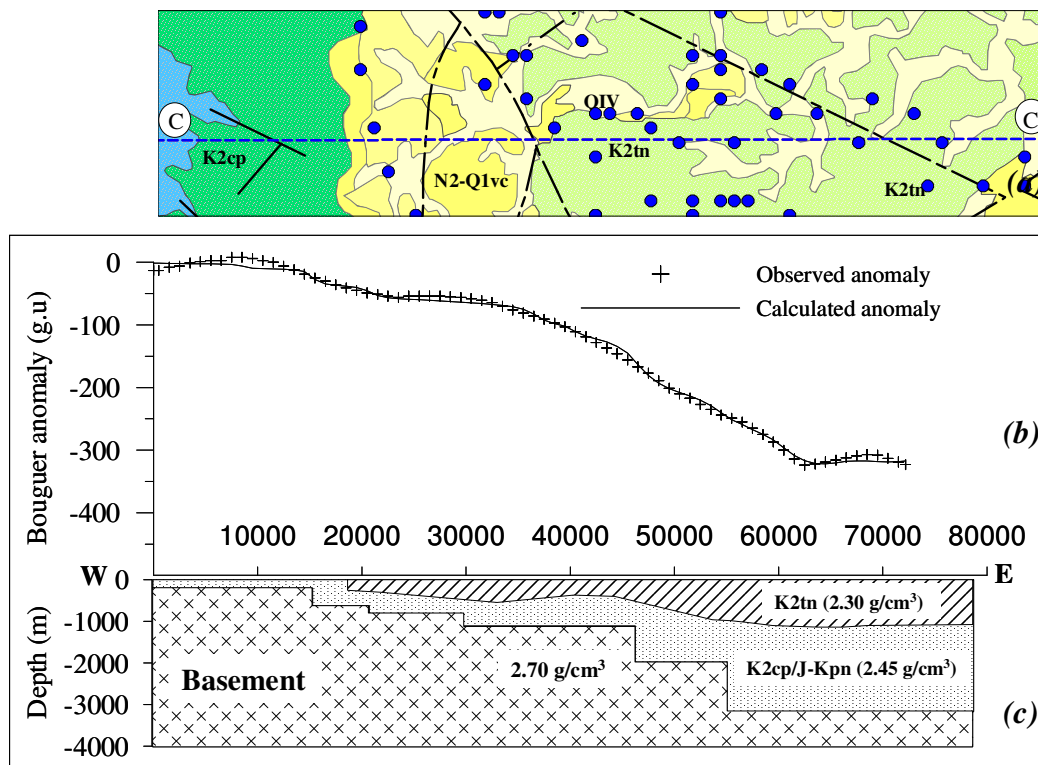


Figure 3.9 (a) Surface geological map in vicinity of line CC'  
 (b) Gravity anomaly on line CC'  
 (c) Geophysical model on line CC'

A decrease of Bouguer anomaly from a constant value of about 0 g.u. on the western end of the profile to -324 g.u. on the eastern end of the profile with steps of decrease around distances 20,000, 29,000 and 55,000 meters were clearly observed, as shown in Figure 3.9 (b). The surface geology in vicinity of line BB' is shown in Figure 3.9 (a). Geological faults of northwest-southeast and northeast-southwest trending were also reported between distances 20, 000 and 40,000 meters and at 70,000 meters.

An increase in thickness of basin sediments of Cretaceous age from 200 meter at distance 0 meters on the western end to 3,200 meters on the eastern end with steps of change in thickness of basin sediments between distances 15,000 and 55,000 meters was modeled to explain the decrease of Bouguer anomaly on line CC' (Figure 3.9 (b)). Similarly, a salt layer of less than 1,000 meters thick was modeled in the upper part of basin sediments to conform to subsurface geology of the study area.

#### **3.3.4 Line DD' (18°12'N)**

Gravity anomaly and subsurface geological model of line DD' are shown in Figure 3.10 (b) and (c). Line DD' is at latitude 18°12'N and longitudes 102°21'E to 103°00'E and its length is about 70 kilometers. A decrease of Bouguer anomaly from a constant value of about 0 g.u. on the western end of the profile to -390 g.u. on the eastern end of the profile with steps of decrease around distances 15,000, 23,000, and 35,000 meters were clearly observed, as shown in Figure 3.10 (b). The surface geology in vicinity of line BB' is shown in Figure 3.10 (a), and geological faults were reported between distances 25, 000 and 45,000 meters.

An increase in thickness of basin sediments of Cretaceous age from 200 meter at distance 0 meters on the western end to 4,000 meters on the eastern end with steps of change in thickness of basin sediments between distances 16,000 and 65,000 meters was modeled to explain the gentle decrease of Bouguer anomaly on line DD' (Figure 3.10 (b)). Similarly, a salt layer of less than 1,000 meters thick was modeled in the upper part of basin sediments to conform to subsurface geology of the study area.

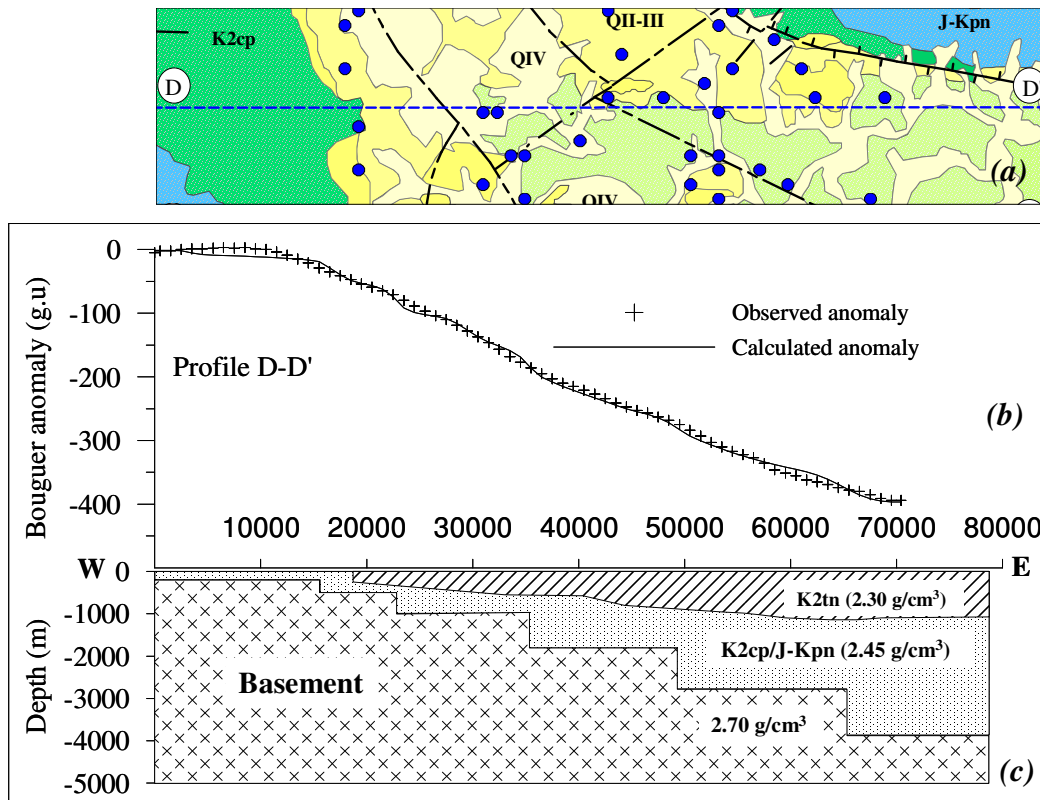


Figure 3.10 (a) Surface geological map in vicinity of line DD'  
 (b) Gravity anomaly on line DD'  
 (c) Geophysical model on line DD'

### 3.3.5 Line EE' (18°16'N)

Gravity anomaly and subsurface geological model of line EE' are shown in Figure 3.11 (b) and (c). Line DD' is at latitude 18°16'N and longitudes 102°21'E to 103°00'E and its length is about 70 kilometers. A decrease of Bouguer anomaly from 0 g.u. on the western end of the profile to -400 g.u. on the eastern end of the profile with steps of decrease around distances 17,000, 29,000, 44,000 and 62,000 meters were clearly observed, as shown in Figure 3.11 (b). The surface geology in vicinity of line BB' is shown in Figure 3.11 (a). Northeast-southwest trending geological faults were reported between distances 20,000 to 55,000 meters

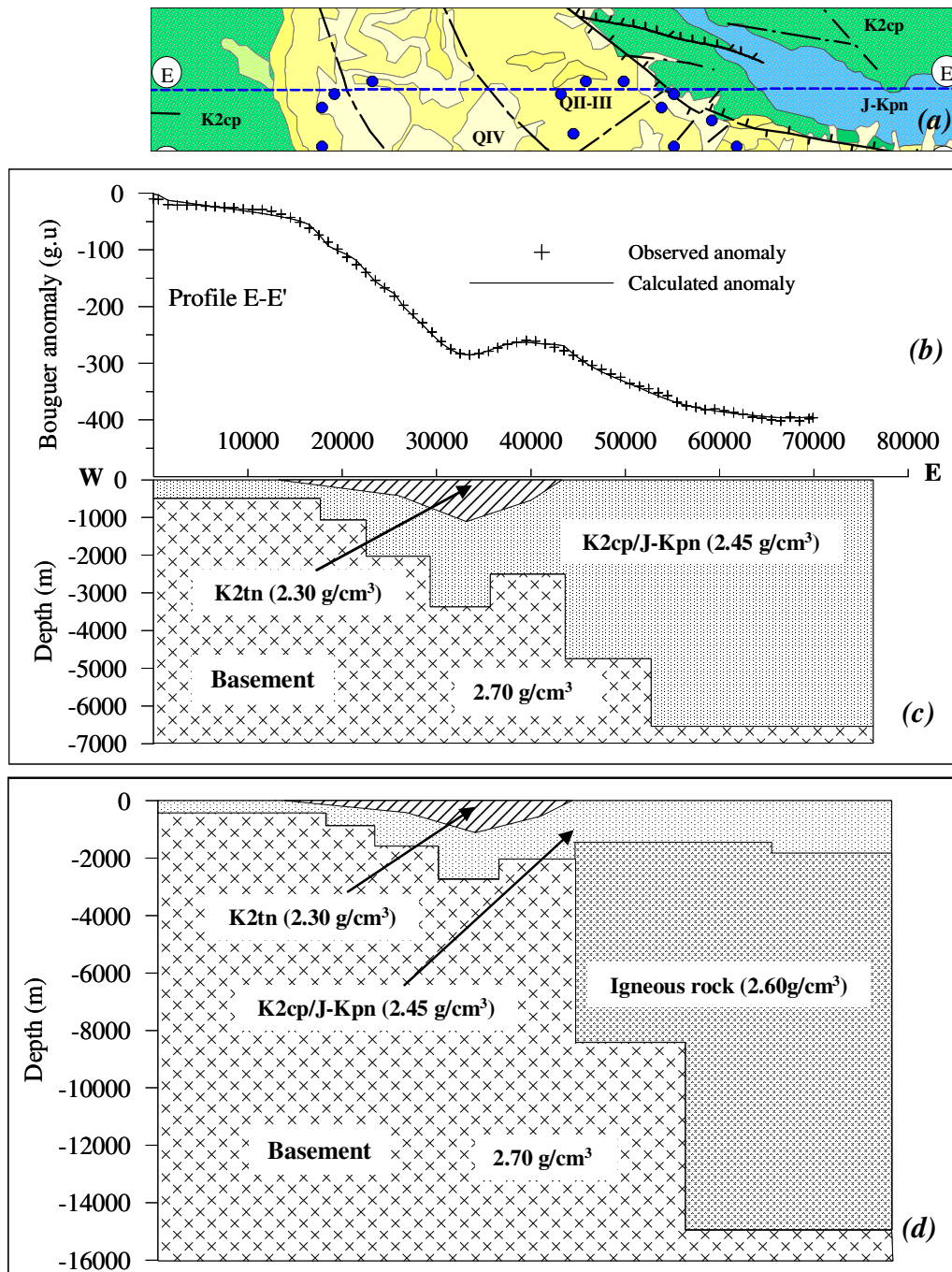


Figure 3.11 (a) Surface geological map in vicinity of line EE'  
 (b) Gravity anomaly on line EE'  
 (c) The first geophysical model on line EE'  
 (d) The second geophysical model on line EE'

An increase in thickness of basin sediments of Cretaceous age from 200 meter at distance 0 meters on the western end to 6,500 meters on the eastern end with steps of change in thickness of basin sediments between distances 17,000, 23,000, 29,000, 36,000, 44,000, and 53,000 meters was modeled to explain the gentle decrease of Bouguer anomaly on line EE' (Figure 3.11 (c)). However, a salt layer is also about 1,000 meters thick was modeled in the upper part of basin sediments between distances 10, 000 and 43,000 meters, as shown in Figure 3.11 (b).

Because the thickness of basin sediment of Cretaceous age in eastern end of line EE' is so great, 6,500 meters thick, it is unlikely that the density of Cretaceous sediment will remain constant at  $2.45 \text{ g/cm}^3$ . However, subsurface rock of low density (less than  $2.70 \text{ g/cm}^3$ ) is required to explain low Bouguer anomaly at the eastern end, and two possible models are proposed. The first model is Cretaceous sediment of  $2.45 \text{ g/cm}^3$  and 6,500 meters thick (Figure 3.11 (c)) in a complex tectonic regimes of which the area experienced compressional and tensional stresses. The second model is intrusion of subsurface igneous rock of  $2.60 \text{ g/cm}^3$  and 15,000 meters thick (Figure 3.12 (d)). This is because plutonic rocks were reported in the north-east of the present study area (Charusiri *et al.*, 2000). However, addition geological information should be acquired and used as constraints in deciding the most possible model of this area.

The map of depth to basement of Vientiane basin obtained from the present gravity modeling on lines AA', BB', CC', DD' and EE' (model-1) as shown in Figure 3.12. It can be observed that the depth to basement increases eastward with its deepest part in the northeastern region. In addition, a change in the course of the Nam Ngum River from North-South to West-East direction may probably associate with a rise of the basement in the middle part of the study area.

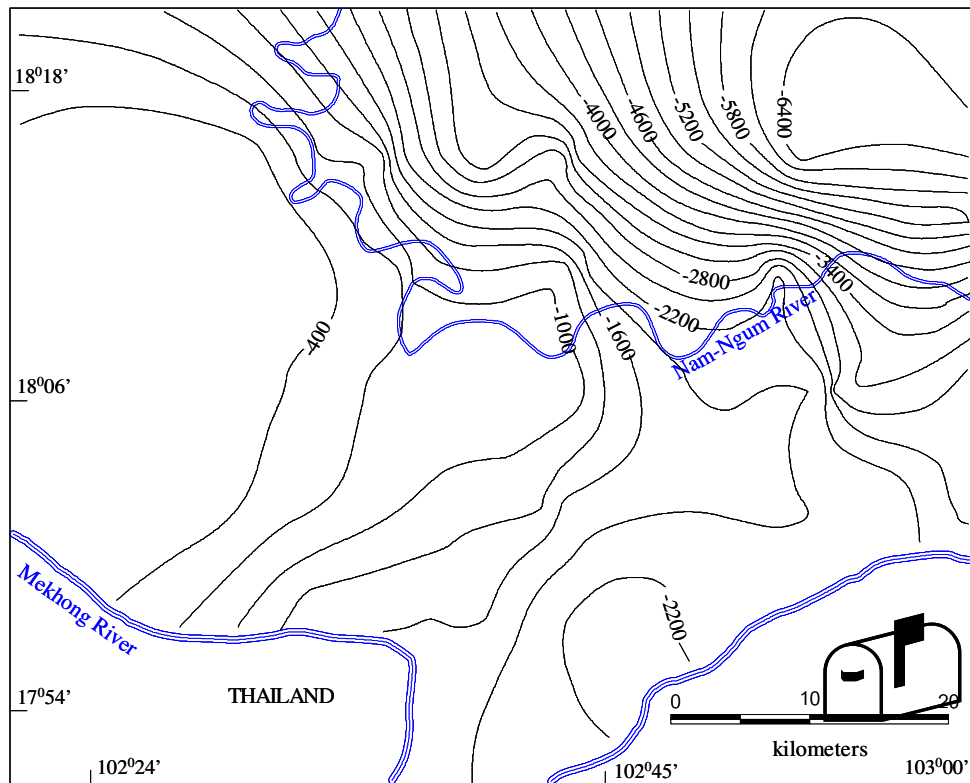


Figure 3.12 Contour map of the depth to basement of Vientiane basin  
(Contour interval of 300 meters)

### 3.4. Electrical measurement in Xaithani district

All together 30 vertical electrical sounding points were conducted in the study area in order to determine geological structure at a shallow depth.

Resistivity sounding curves obtained from present work can be classified into two groups. In general, the apparent resistivity curve of the first group, Group-I, is of “H” type ( $\rho_1 > \rho_2 < \rho_3$ ), while that of the second group, Group-II, is of “Q” type ( $\rho_1 > \rho_2 > \rho_3$ ) as shown in Figure 3.13 (a) and (b).

Generally, apparent resistivity is greater than 100 ohm-m at small electrode spacing and decreases to the asymptotic value of 10 ohm-m at larger current electrode spacing. However, at some sounding stations, apparent resistivity of the ground tends to increase again at very large electrode spacing.

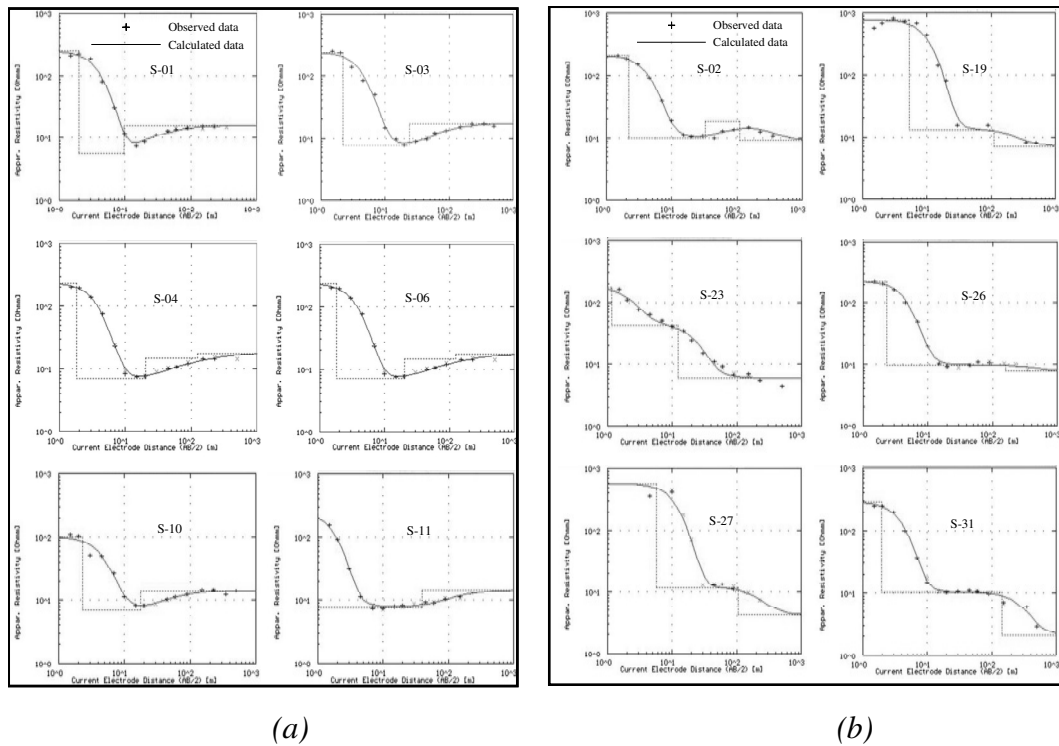


*Figure 3.13* VES-curves obtained from Xaithani district (a) Group-I at sounding stations of S01, S03, S04, S06, S-10, and S-11,(b) Group-II at sounding stations of S-02, S-19, S23, S-26, S-27, and S31

In addition, contour maps of apparent resistivity at half current electrode spacing of 1.5 m, 10 m, 20 m, 30 m, 45 m, 60 m, 90 m, 150 m, 225 m and 350 m as shown in Figures 3.15 (a) and (b). It can be observed that high apparent resistivity of greater than 100 ohm-m appears at small current electrode spacing at 1.5 m and some parts of Xaithani district at electrode spacing of 10 m, 20 m, 30 m and 45 m (Figure 3.15 (a)). However, apparent resistivity of 30 to 100 ohm-m was observed in the southwestern of Xaithani district at electrode spacing of 90 m, 150 m, and 350 m as shown in Figure 3.15 (b).

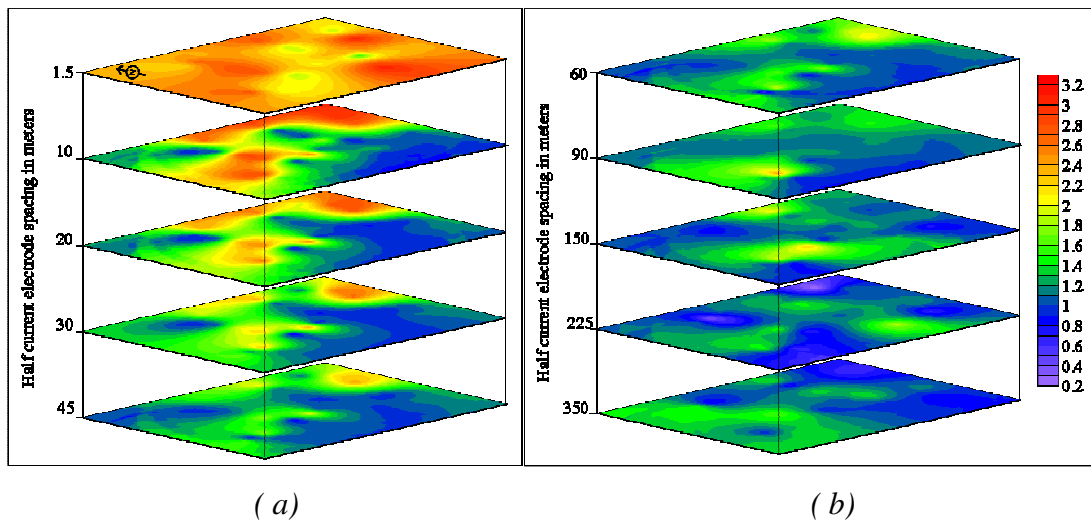


*Figure 3.14* Apparent resistivity maps of Xaithani district at different half current electrode spacing (Contour is in logarithmic value of apparent resistivity)

Sounding curves at S-01, S-03, S-04, and S-06, S-10, and S-11 (Figure 3.13 (a)) are examples of Group-I. Generally, three-layered earth was modeled from these curves with the following parameters; resistivity of greater than 100 ohm-m and 0.9 to 3.5 meters thick for the top layer, low resistivities range 5.7 to 7.8 ohm-m and 7.6 to 81 meters thick for the second layer, and resistivity of 14.2 to 42.1 ohm-m for the bottom layer. The interpreted resistivity models of all soundings in Group-I are summarized in Table 3.2.

Sounding curves at S-02, S-19, S23, S-26, S-27, and S31, (Figure 3.13 (b)) are examples of the second group. Three-layered earth was also modeled from these curves with the following parameters; resistivity of greater than 100 ohm-m and the thickness of 1.2 to 5.7 meters for the top layer, resistivity varies from 9.8 ohm-m to 42.9 ohm-m with thickness ranges 11 meters to 154.4 meters for the second layer, and resistivity of less than 10 ohm-m for the bottom layer. The interpreted resistivity models of all soundings in Group-II are summarized in Table 3.2.

Table 3.2: The interpret resistivity models of sounding points of each groups, where  $\rho_i$  and  $d_i$  are resistivity and depth of  $i^{\text{th}}$  layer.

Group	Stn.	Layer 1		Layer 2		Layer 3		Layer 4	
		$\rho_1(\Omega\text{m})$	$d_1(\text{m})$	$\rho_2(\Omega\text{m})$	$d_2(\text{m})$	$\rho_3(\Omega\text{m})$	$d_3(\text{m})$	$\rho_4(\Omega\text{m})$	$d_4(\text{m})$
I	S01	252.7	0	5.7	2.0	15.9	9.6	-	-
	S03	209.2	0	7.7	2.2	17.0	24.0	-	-
	S04	235.4	0	7.0	1.8	14.7	20.4	17.7	123.5
	S06	99.2	0	7.1	2.3	14.2	17.7	-	-
	S08	76.7	0	5.4	2.2	44.0	64.2	-	-
	S09	120.8	0	8.8	0.5	56.9	22.0	-	-
	S10	325.9	0	7.5	3.5	42.1	84.5	-	-
	S11	256.0	0	7.8	0.9	14.6	39.3	-	-
	S12	748.2	0	10.4	1.0	19.9	139.7	-	-
	S14	583.5	0	22.4	10.9	68.5	132.3	-	-
	S15	671.3	0	340.7	5.0	18.8	19.4	36.4	158.3
	S16	317.4	0	10.1	1.3	9.3	6.9	14.6	18.1
	S21	212.9	0	9.8	0.7	14.2	34.8	-	-
	S22	160.2	0	11.9	1.1	19.2	42.0	-	-
S25	737.9	0	9.3	1.1	82.9	100.8	-	-	
II	S02	209.2	0	10.1	2.2	18.5	32.5	9.3	109.3
	S05	190.9	0	11.6	2.5	-	-	-	-
	S07	167.2	0	643.8	1.8	8.0	11.4	-	-
	S13	488.1	0	226.4	2.3	10.8	13.6	-	-
	S18	365.9	0	48.2	4.5	11.9	38.8	-	-
	S19	770.9	0	13.2	5.4	7.1	109.8	-	-
	S23	171.1	0	42.9	1.2	6.1	12.1	-	-
	S24	997.6	0	38.8	9.2	44.2	89.5	5	122.1
	S26	228.5	0	9.8	2.3	7.9	156.6	-	-
	S27	579.3	0	11.6	5.7	4.1	105.2	-	-
	S28	1271.7	0	24.0	12.0	1.8	111.7	-	-
	S29	182.2	0	1554.7	2.3	8.2	8.9	-	-
	S30	489.1	0	9.6	10.0	8.4	114.1	-	-
	S31	292.0	0	10.2	2.0	2.1	142.8	-	-
S32	67.4	0	8.4	0.7	20.6	7.8	4.4	30.7	

True resistivity maps at different depths obtained from interpretation of VES curves are shown in Figures.3.15 (a) and (b). These maps showed high resistivity of greater than 100 ohm-m at ground surface and moderate resistivities of 40 to 100 ohm-m in southwestern part of the study area at 5 m and 10 m depths. Low resistivity

of less than 12 ohm-m was observed in most part of Xaithani district at depths 15 m to 80 m. Moderate resistivities of 25 to 60 ohm-m appear in southwestern part of Xaithani district at 80 m, 100 m and 150 m depths (Figure 3.15 (b)).

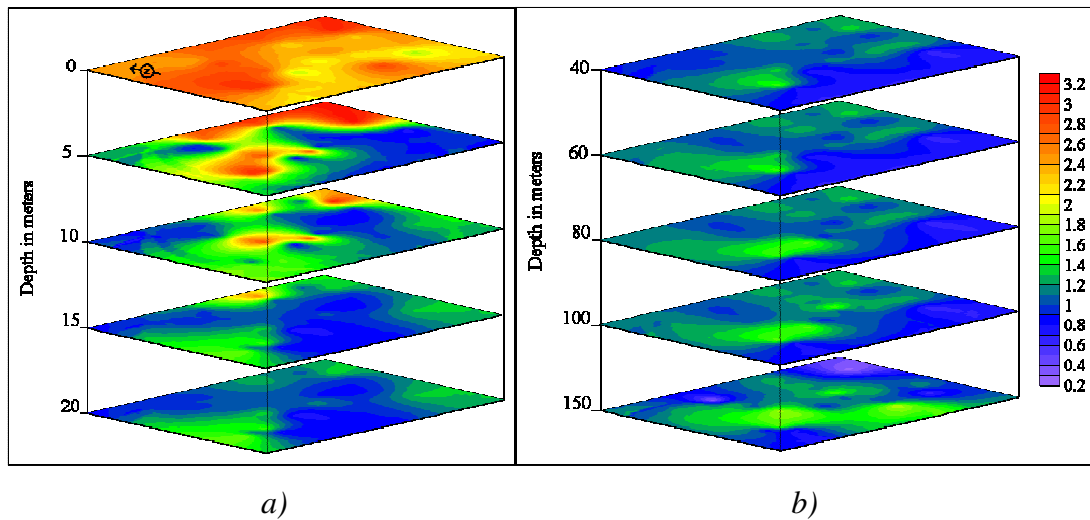


Figure 3.15 True resistivity contour maps of Xaithani district at different depths. (Contour is logarithmic value of true resistivity)

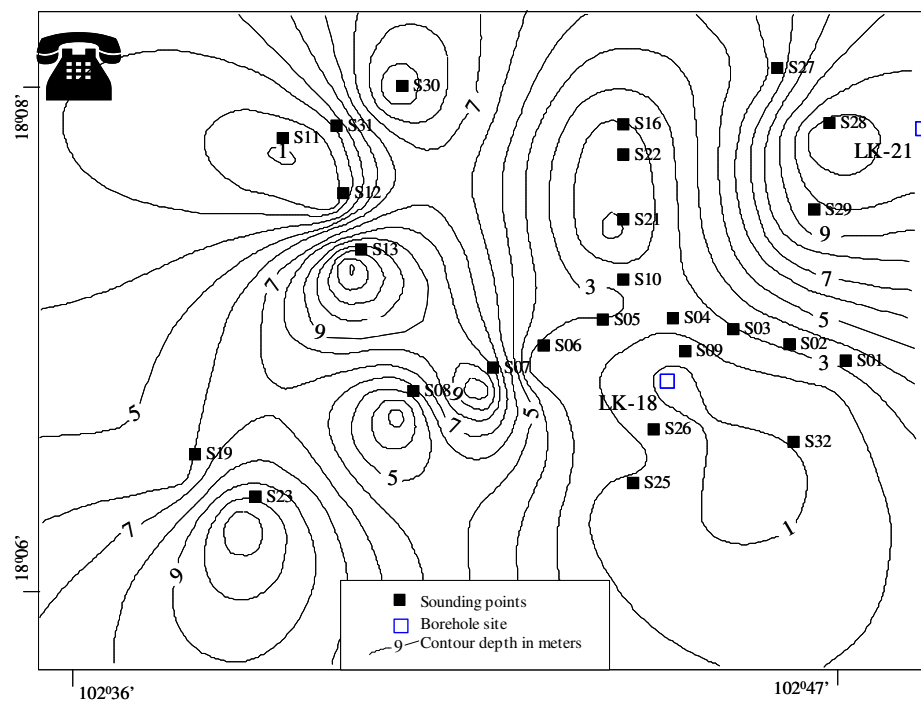


Figure 3.16 Contour map of the depth to the top of the conductive layer (Contour interval of 1 meter)

Based on the VES results a layer of low resistivity less than 24 ohm-m was observed in almost every sounding point. The depth to this conductive layer was displayed as contoured maps in Figure 3.16. This conductive layer is at very shallow depth, 0.7 to 13.6 meters below ground surface, except two sounding points at S-18 and S-24 where depths to this conductive layer are at 39 meters and 112 meters respectively.

#### 3.4.1. Comparison of resistivity models with geological logs

The resistivity models of sounding points S26 and S27 were compared with geological logs of wells Lk18 and Lk21 respectively (Figures.3.17 and 3.18). Its purpose is to determine a correlation between lithological information and resistivity model.

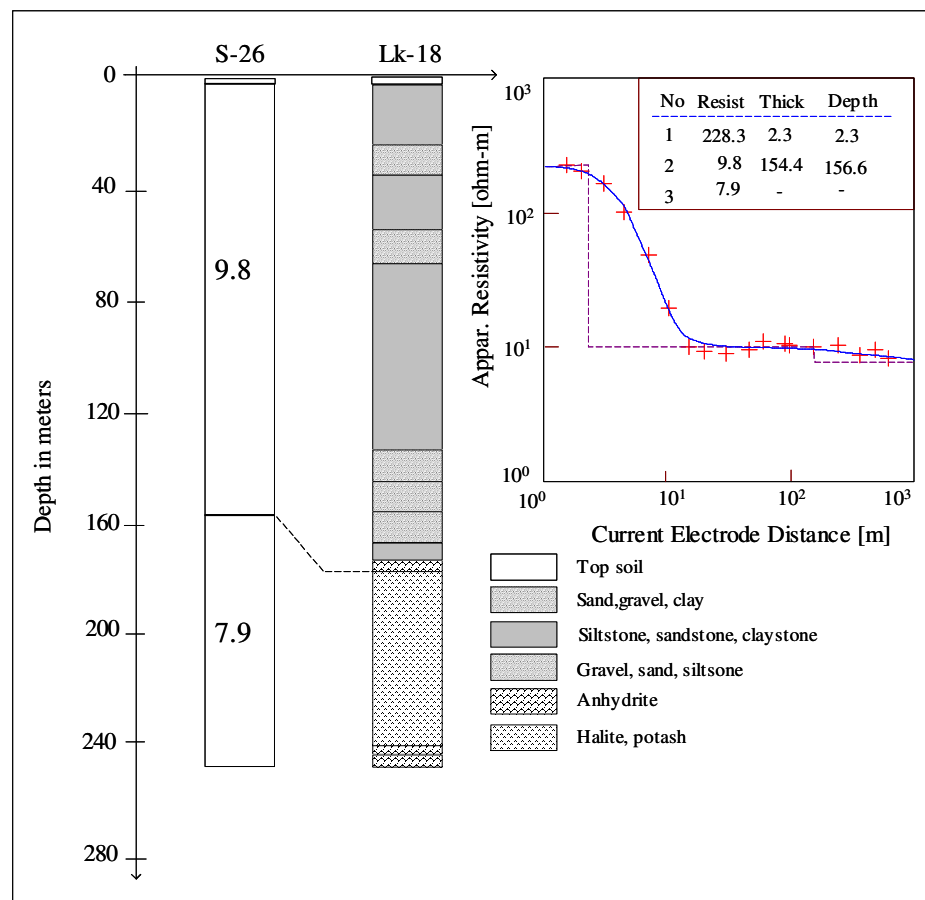


Figure 3.17 Correlation of VES-result at sounding point S-26 with the known lithology of well Lk-18

Three-layer earth model was obtained from resistivity interpretation of sounding point S26. The first layer of 228.5 ohm-m and 2.3 meters thick corresponds with the top soil of well number Lk-18. The second layer of 9.8 ohm-m in resistivity model at 2.3 to 156.6 meters depth corresponds with claystone, siltstone, and sandstone layers at 2.5 to 179.6 meters depth of this well. The bottom layer of resistivity model, 7.9 ohm-m at 156.6 meters depth, corresponds with halite salt layer at depths 179.6 to 250.5 meters with a thin layer of anhydrite interbedded at depths of 243.7 to 247.9 meters (Figure 3.17)

Three-layer earth model was also obtained from resistivity interpretation of sounding point S27. The first layer of 579.3 ohm-m and 5.7 meters thick in resistivity model corresponds with the top soil of well Lk-21. The second layer of 11.6 ohm-m in resistivity model at 5.7 to 105.2 meters depth corresponds with claystone, siltstone, and sandstone layers at 4.8 to 152 meters depth. The bottom layer of resistivity model of 4 ohm-m at 105.2 meters depth corresponds with halite salt layer at 152 to 620 meters depth (Figure 3.18).

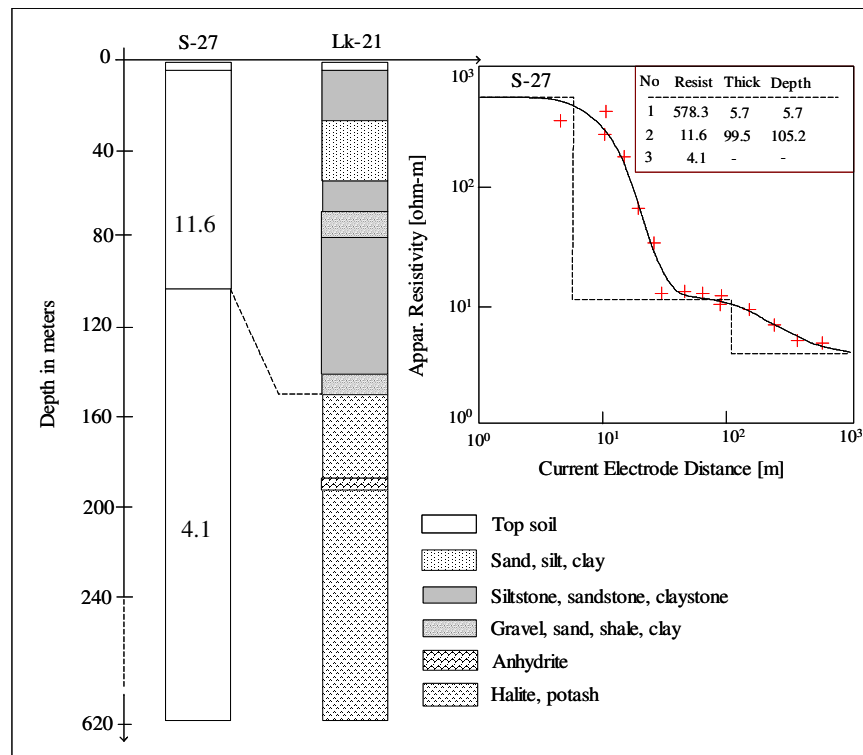


Figure 3.18 Correlation of VES-result at sounding point of S-27 with the known lithology of well Lk-21

It is clearly observed from this study that shallow sediments in Vientiane basin, down to 620 m, are electrically conductive, 4 to 12 ohm-m. The sediments are thick layers of sand, silt, clay and halite salt. The resistivity of halite is a little lower than that of sand, silt and clay, 4 to 8 ohm-m for halite salt compared with 10 to 12 ohm-m for sand, silt and clay. These conductive layers will certainly limit the penetrating depth of electrical resistivity method conducted in Vientiane basin.

#### 3.4.2. Potential area for groundwater in the study area

Resistivity Map of bottom layer obtained from sounding interpretation is shown in Figure 3.19. It can be observed that the resistivity of the bottom layer in the eastern, northern and the western parts of the study area, is less than 30 ohm-m, whereas that in the southern part of the study area is greater than 30 ohm-m.

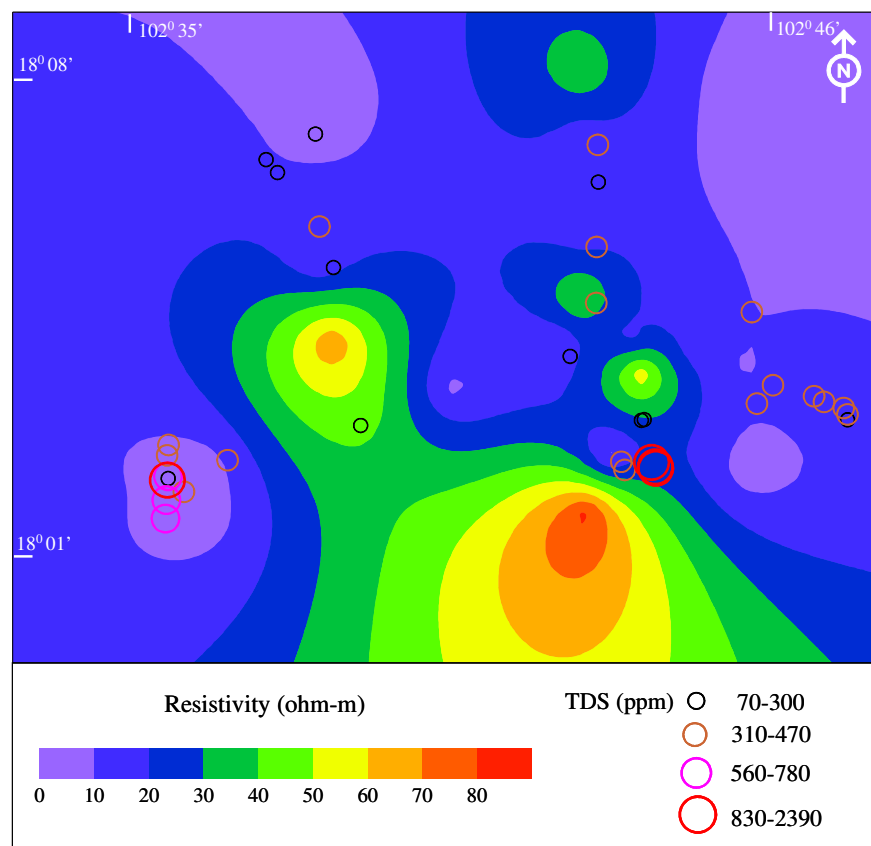
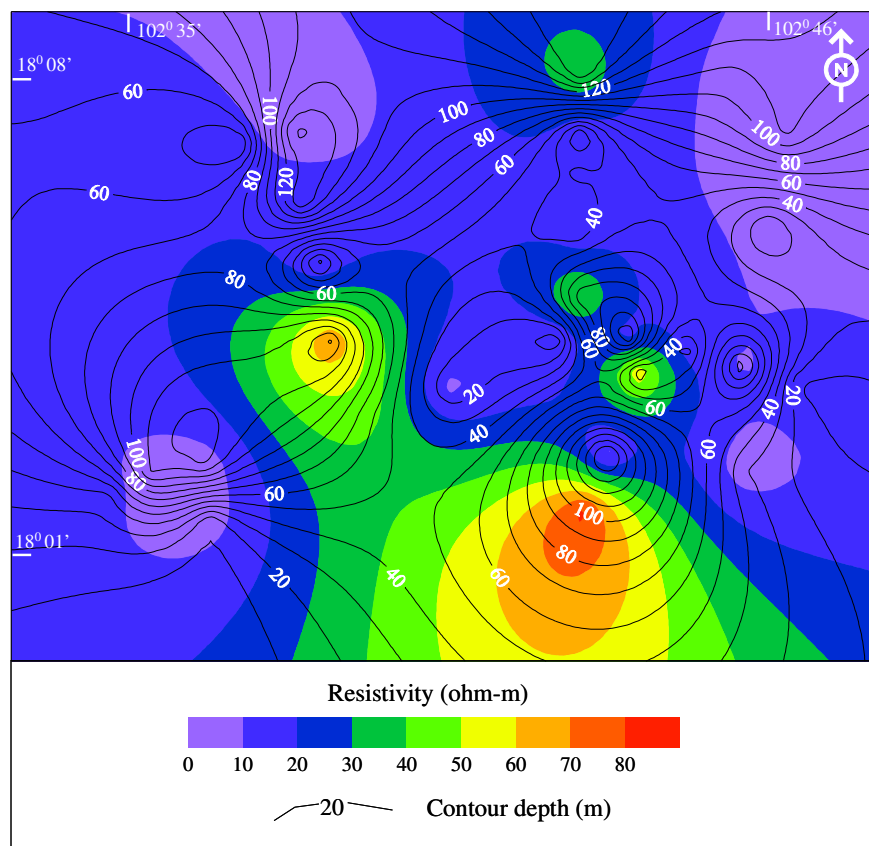


Figure 3.19 Resistivity contour maps of Xaithani district correlated to TDS values

This high resistivity zone is likely to continue north-westward into the central part of the study area. This area is considered from the present study as the potential area for fresh groundwater. This interpretation is confirmed by the TDS measurement conducted on 35 water samples at 30 to 40 meters depth wells in the study area. It clearly observed that high TDS values are outside this high resistivity zone of fresh groundwater. In addition, depth to bottom layer ranges from 30 to 130 meters for areas of good quality groundwater, as shown in Figure 3.20.



*Figure 3.20* Resistivity contour maps with contour depth to the bottom layer